ARTICLES
PUBLISHED ONLINE: 3 FEBRUARY 2013 | DOI: 10.1038/NCHEM.1565
nature chemistry

Volume-conserving *trans*–*cis* isomerization pathways in photoactive yellow protein visualized by picosecond X-ray crystallography

Yang Ouk Jung[1,2], Jae Hyuk Lee[2], Joonghan Kim[2], Marius Schmidt[3], Keith Moffat[4,5], Vukica Šrajer[5] and Hyotcherl Ihee[1,2]*

***Trans*-to-*cis* isomerization, the key reaction in photoactive proteins, usually cannot occur through the standard one-bond-flip mechanism. Owing to spatial constraints imposed by a protein environment, isomerization probably proceeds through a volume-conserving mechanism in which highly choreographed atomic motions are expected, the details of which have not yet been observed directly. Here we employ time-resolved X-ray crystallography to visualize the isomerization of the *p*-coumaric acid chromophore in photoactive yellow protein with a time resolution of 100 ps and a spatial resolution of 1.6 Å. The structure of the earliest intermediate (I_T) resembles a highly strained transition state in which the torsion angle is located halfway between the *trans*- and *cis*-isomers. The reaction trajectory of I_T bifurcates into two structurally distinct *cis* intermediates via hula-twist and bicycle-pedal pathways. The bifurcating reaction pathways can be controlled by weakening the hydrogen bond between the chromophore and an adjacent residue through E46Q mutation, which switches off the bicycle-pedal pathway.**

The ability to convert light into molecular action is indispensable to many forms of life, as in, for example, light-activated signal transduction in mobile bacteria and vision in animals. These tasks are accomplished by signalling photoreceptor proteins in which light activation often triggers geometrical isomerization of a prosthetic chromophore group, typically a π-conjugated organic molecule buried within the host protein. The isomerization pathway in the gas and solution phases, where the chromophore is free from host constraints, is thought to proceed via a mechanism that involves a one-bond flip[1] (Fig. 1a). When the chromophore is embedded in a cavity within a photoreceptor, this mechanism may no longer hold because interactions with the surrounding side chains of the protein, including hydrogen-bond interactions and steric constraints, severely restrict the conformational mobility of the chromophore[1,2]. Instead, volume-conserving isomerization mechanisms[3,4] should be considered when the pathway of isomerization proceeds along a trajectory that minimizes the volume swept out by the atoms of the chromophore[5] (Fig. 1a). For example, molecular dynamics (MD) simulations of the retinal chromophore in rhodopsin suggest that it isomerizes via a volume-conserving bicycle-pedal (BP) mechanism[2,6–8]. Similarly, infrared spectroscopic[9–12] and crystallographic studies[5,13–17] of the *p*-coumaric acid (pCA) chromophore of photoactive yellow protein (PYP) suggest the BP mechanism. An alternative volume-conserving mechanism, the hula twist (HT)[1], was observed in various small-molecule and biomacromolecular systems[18], but not directly in PYP[5]. Both BP and HT isomerization involve correlated motion along numerous internal coordinates, but the highly choreographed atomic motion required by each mechanism had not been observed experimentally.

PYP is a photoreceptor whose activation is believed to lead to negative phototaxis of the bacterium *Halorhodospira halophila*[19]. Owing to its small size, stability and well-ordered crystals[20], PYP provides an excellent model system for investigating structure–function relationships in photoreceptor proteins. The pCA chromophore occupies a cavity inside the protein (Fig. 1). It is anchored covalently at one end to Cys69 through a thioester bond, and forms hydrogen bonds with the side chains of Tyr42 and Glu46 and the backbone amide of Cys69. Absorption of a blue photon triggers photoisomerization of pCA, which drives a fully reversible photocycle in which the signalling state persists long enough to be recognized by the organism[19]. This photocycle has been investigated extensively by spectroscopy[10–12,21–27] and crystallography[13,16,17,28,29] using cryogenic and time-resolved techniques (Fig. 1d). Ambient-temperature transient-absorption spectroscopy revealed, on a sub-nanosecond time scale, two distinguishable early intermediates, I_0 and $I_0^{\ddagger}$, that evolve into later intermediates I_1 (or pR) and I_2 (or pB)[21,22,25]. According to time-resolved Fourier transform infrared studies[10,11], a ground-state intermediate (GSI) forms on a femtosecond time scale and decays to the ground state (pG) on a picosecond time scale. The structures of these short-lived intermediates remained unclear, as previous time-resolved crystallography studies at ambient temperature[17,28] were done with 5–10 ns resolution, and thus lacked the time resolution required to capture these earliest intermediates. Here, we report results of time-resolved crystallographic experiments with a 100 ps time resolution that track the *trans*-to-*cis* photoisomerization of the pCA for both wild-type PYP (WT-PYP) and its E46Q mutant. Isomerization occurs via a highly distorted intermediate whose reaction trajectory appears to bifurcate along the BP and HT pathways to produce two structurally distinct *cis* intermediates. One of the bifurcating pathways can be blocked by weakening the hydrogen bond from residue 46; the BP pathway is blocked in the E46Q mutant.

[1]Center for Nanomaterials and Chemical Reactions, Institute for Basic Science, Daejeon, 305-701, Republic of Korea, [2]Center for Time-Resolved Diffraction, Department of Chemistry, KAIST, Daejeon, 305-701, Republic of Korea, [3]Physics Department, University of Wisconsin-Milwaukee, Milwaukee, Wisconsin 53201, USA, [4]Department of Biochemistry and Molecular Biology, and Institute for Biophysical Dynamics, The University of Chicago, 929 East 57th Street, Chicago, Illinois 60637, USA, [5]Center for Advanced Radiation Sources, The University of Chicago, 5640 S Ellis Avenue, Chicago, Illinois 60637, USA.
*e-mail: hyotcherl.ihee@kaist.ac.kr

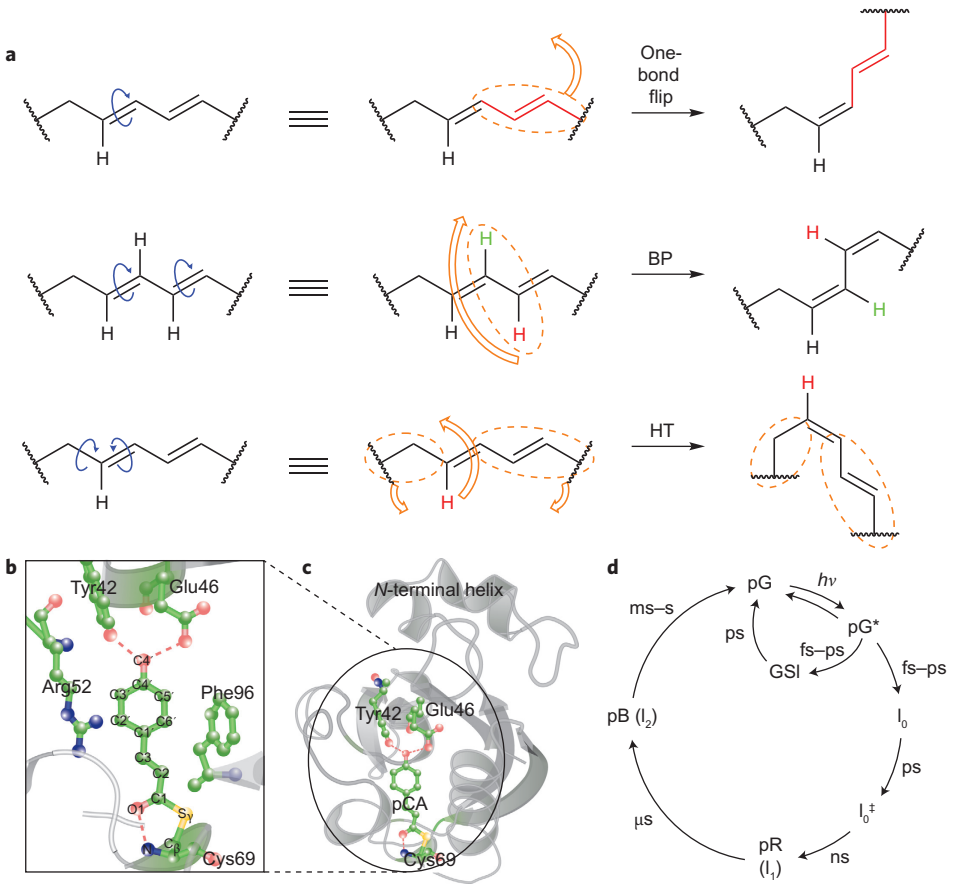

Figure 1 | Isomerization mechanisms and overview of the PYP. a, Schematic description of the three isomerization mechanisms discussed in this work. The one-bond flip is a simple *trans* ↔ *cis* isomerization around one double bond. The BP process involves the simultaneous rotation of two adjacent double bonds and the HT mechanism involves the simultaneous rotation of adjacent double and single bonds. The bond rotations are shown with blue arrows and the orange arrows show the general movements in space of the circled sections of the molecules. **b**, Close up of the pCA chromophore and neighbouring residues (the dashed lines denote hydrogen-bond interactions). Carbon, oxygen, sulfur and nitrogen atoms are shown in green, red, yellow and blue, respectively. **c**, Structure of the protein (ribbon) and the pCA (ball and stick) in the chromophore binding pocket. **d**, Photocycle and corresponding kinetics, as derived from time-resolved spectroscopy measurements at ambient temperature[10–12,25,49].

Results and discussion

Time-dependent density maps. Electron-density maps of the chromophore binding pocket for representative time delays (−20 ns, 100 ps, 3.16 ns and 1 μs for WT, and −20 ns, 100 ps and 31.6 ns for E46Q) are shown in Fig. 2 (for a complete time series see Supplementary Figs S1–S3 and Supplementary Movies S1–S3). Superposition of magenta–green colour-coded (thresholdless) maps[30] for the ground state (magenta) and the extrapolated photoactivated state (green) are shown for the chromophore binding pocket in both front (Fig. 2a) and side views (Fig. 2b) for WT-PYP. These two colours blend to white where they overlap and the magenta-to-green colour gradient indicates the direction of atomic motions. The −20 ns time point provides a control in which the X-ray pulse arrives in advance of the laser pulse and therefore records the structure of the resting dark state. At the earliest time delays, structural changes are confined largely to the chromophore binding pocket (see Supplementary Figs S1–S3). The magenta–green maps reveal correlated motions of the pCA chromophore and the surrounding protein as the chromophore undergoes isomerization. Yellow arrows and circles in Fig. 2 indicate motions at each time point. For example, the WT-PYP 100 ps side view in Fig. 2b depicts a highly twisted structure in which the phenolate ring has shifted to the left, the C2–C3 atoms have shifted to the right and the carbonyl O1 has rotated out of the plane of the chromophore. Also, in the 100 ps front view in Fig. 2a the movement of the carbonyl O1 is clearly visible and the movements of the surrounding residues are apparent. That the Tyr42 and Glu46 side chains follow the phenolate suggests that their hydrogen-bond network with the pCA remains intact. As a result of their close-packed arrangement, Arg52, Phe96 and Met100 follow the motion of the phenolate and C2–C3 atoms. In the 3.16 ns front view of WT-PYP in Fig. 2a, the carbonyl O1 has rotated to the opposite side of the tail of the chromophore, as in cryotrapped structures reported previously (I_0[13], PYP_B[14] and I_{CP}[15]). In the 1 μs map, the movement of the sulfur atom for the pR_{CW} intermediate is visible, as reported previously[17]. In the case of the E46Q mutant (Fig. 2c,d), similar movements of pCA and nearby residues at 100 ps were observed. In the nanosecond time regime represented by the 31.6 ns map, the movement of the phenolate ring in the E46Q mutant is more pronounced than that in WT, but some movements (such as the rotation of the carbonyl O1 on the opposite side of the tail of the chromophore) are missing. Also, the movements are delayed relative to those in WT-PYP. This provides direct, qualitative evidence that the kinetics and intermediates in E46Q differ from those in WT-PYP. Visual inspection of the time-dependent electron-density maps provides useful, but nevertheless qualitative, structural insights into the reaction mechanism. In particular, individual maps probably contain a mixture of multiple intermediates. To elucidate the

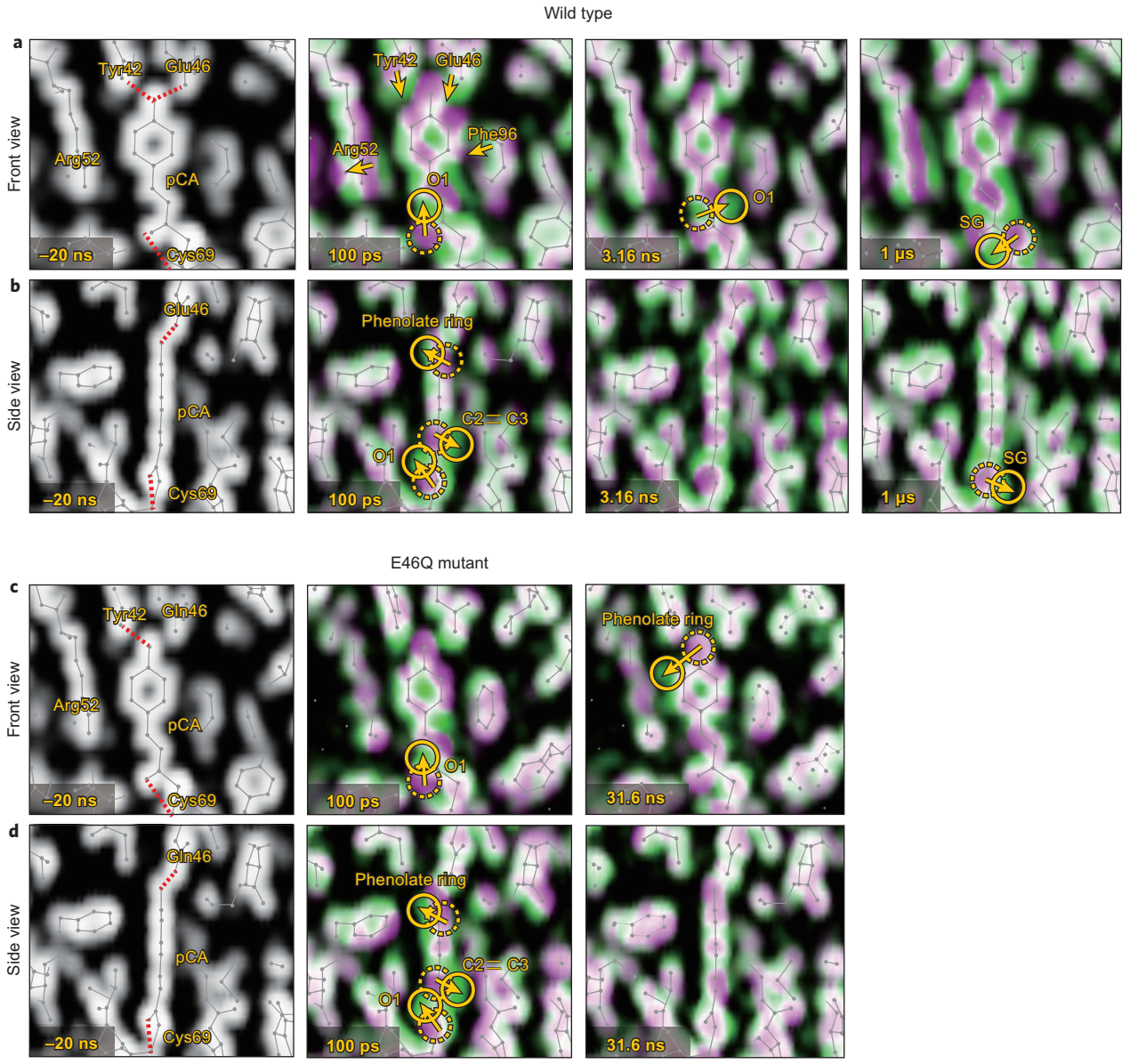

Figure 2 | Time-resolved electron-density maps of pCA in the chromophore binding pocket. a–d, Superposition of thresholdless electron-density maps[30] for the ground state (magenta) and extrapolated photoactivated state (green). The two colours blend to white where they overlap, the direction of molecular motion follows the magenta-to-green colour gradient and the solid and dotted circles indicate the appearance and disappearance of density, respectively. **a**,**c**, Front views of the chromophore binding pockets for WT-PYP (**a**) and E46Q-PYP (**c**). **b**,**d**, Side views of WT-PYP (**b**) and E46Q-PYP (**d**). For clarity, only 100 ps, 3.16 ns and 1 µs maps for the WT (or 100 ps and 31.6 ns maps for the E46Q mutant) are shown (the complete time series is given in Supplementary Figs S1–S3 and Supplementary Movies S1–S3).

structures of transient intermediates involved in the reaction mechanism requires quantitative analysis, as described in the next section.

Extracting intermediate structures and determining kinetics. To determine the time-independent structures of intermediates and the associated kinetics required to reproduce the entire series of experimental time-dependent electron-density maps, we analysed difference electron-density maps using singular value decomposition (SVD) and further kinetic analysis (see the Supplementary Information for details)[31]. The analysis of WT-PYP density maps recovered three time-independent electron-density maps, which suggests three intermediate states and two apparent relaxation times. The electron-density map extrapolated to 100% photoactivation (see the Supplementary Information) for the first intermediate state (Fig. 3a) is described well by a single homogeneous structure. In contrast, the map for the second state (Fig. 3b) is structurally heterogeneous, which suggests a mixture of two distinct intermediate structures that arise from bifurcation of the earlier structure. The map for the third intermediate state (Fig. 3c) is also a mixture of two structures, one of which is one of the two structures of the second intermediate state. The four structures apparent in these three time-independent electron-density maps were refined against these maps via extrapolated refinement[28] (see the Supplementary Information). We denote these four intermediate structures as I_T (intermediate with twisted structure), I_{CT} (intermediate with *cis*-twisted structure), pR_1 and pR_2. More specifically, the maps associated with the first, second and third intermediate states were used to refine the I_T, $I_{CT} + pR_1$ and $pR_1 + pR_2$ structures, respectively, and they are shown in

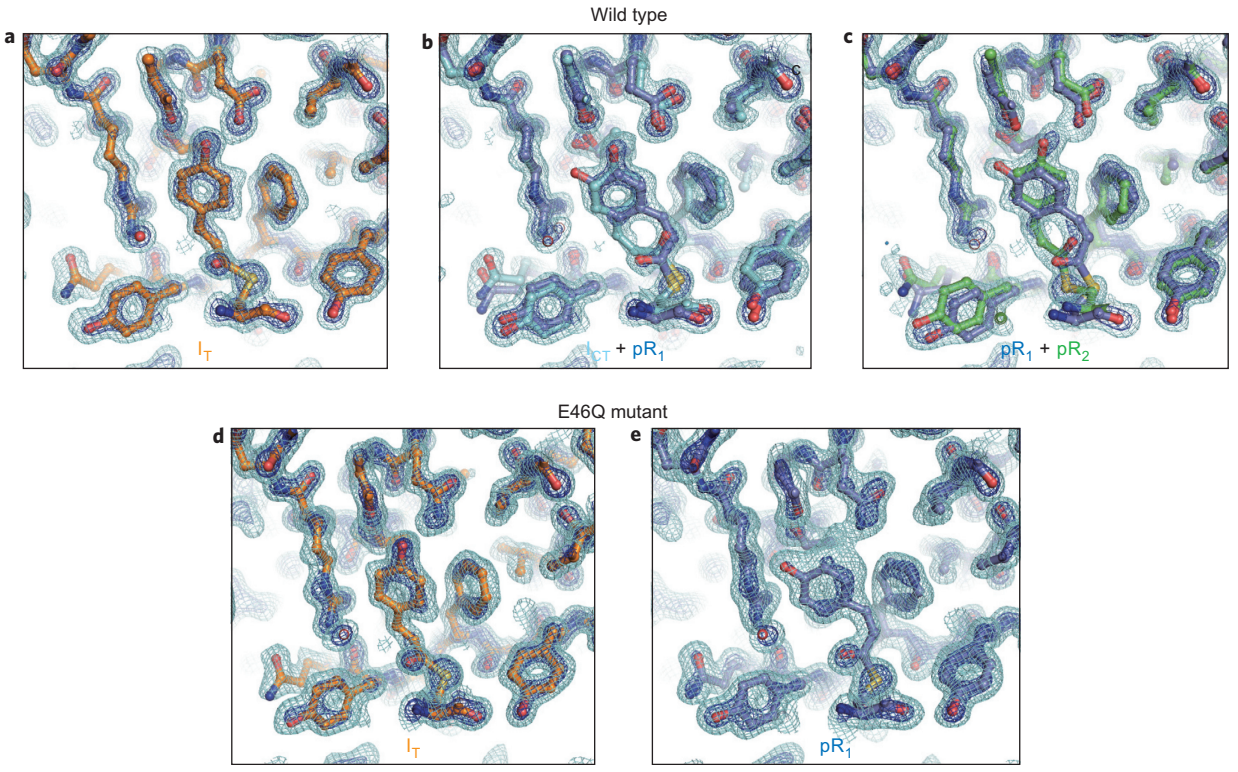

Figure 3 | Time-independent intermediates for WT-PYP and E46Q-PYP recovered from the SVD analysis of time-dependent difference electron-density maps. a–e, Three time-independent electron-density maps were recovered for WT-PYP (**a–c**) and two for E46Q-PYP (**d**,**e**). The densities shown were extrapolated to 100% photoactivation (see the Supplementary Information). The surfaces are contoured at $+1\sigma$ (cyan) and $+3\sigma$ (blue), where σ denotes the r.m.s.d. of electron density. The first (**a**), second (**b**) and third (**c**) WT-PYP intermediates (extracted from SVD analysis of experimental WT-PYP difference electron-density maps collected at ESRF) were modelled with I_T, $I_{CT} + pR_1$ and $pR_1 + pR_2$, respectively. The first (**d**) and second (**e**) E46Q-PYP intermediates (extracted from E46Q-PYP difference maps collected at APS) were modelled with I_T and pR_1, respectively. The structures that correspond to each map are superimposed to the map with the colour coding I_T (orange), I_{CT} (cyan), pR_1 (dark blue) and pR_2 (green).

Fig. 3a–c. The pR_1 structure was refined independently against both the second and third density maps, and the two refined pR_1 structures have identical geometry (with a root mean square deviation (r.m.s.d.) between the two pR_1 structures of ~0.23 Å). I_T and I_{CT} were unknown prior to this work. I_{CT} is related closely to the intermediate I_{CP} reported previously[17], but is less planar. pR_1 and pR_2 correspond directly to pR_{E46Q} and pR_{CW}[17]. Similar analyses of density maps of the E46Q mutant of PYP resulted in two time-independent density maps, both of which are structurally homogeneous and correspond to I_T (Fig. 3d) and pR_1 (Fig. 3e). Intermediates I_{CT} and pR_2 are therefore absent in the E46Q pathway. Selected structural parameters for the stable dark state and all transient intermediates are shown in Table 1.

To characterize further the kinetics of the transitions between the four intermediate structures, the time-dependent WT-PYP experimental density maps were fitted against density maps generated by a plausible mechanism that involved the intermediate structures I_T, I_{CT}, pR_1 and pR_2. For a reaction mechanism consistent with the time-resolved structural changes (Fig. 4a,c), such posterior analysis[31] (details in the Supplementary Information) yields associated time constants of 1.7 ± 0.5 ns, 3 ± 1 ns and 20 ± 7 ns. In this reaction mechanism, I_T bifurcates into pR_1 (via an HT pathway) and I_{CT} (via a BP pathway) with time constants of 3 ns and 1.7 ns, respectively (I_{CT}:pR_1 ~ 6:4). I_{CT} further decays into pR_2 with a time constant of 20 ns. Other possible mechanisms were tested, but none fit the experimental maps satisfactorily. Posterior analysis against the E46Q-PYP density maps recovered a simple sequential kinetic model in which the first intermediate, I_T, transforms to pR_1 (via an HT pathway) with a time constant of 11 ± 1 ns (Fig. 4b,d).

Table 1 | Geometrical parameters of the pCA chromophore in the ground and intermediate states.

	pG	I_T	I_{CT}	pR_1	pR_2	pB
O1–Cys69 (Å)	2.8	2.9	4.7	3.3	4.1	2.9
O4′–Tyr42 (Å)	2.5	2.6	2.4	3.2	2.8	5.0
O4′–Glu46 (Å)	2.6	2.8	3.3	5.4	3.4	7.8
C1–C2–C3–C1′ (°)	169	85	−1	1	3	−24
Planarity angle (°)	22	85	45	35	45	51

The planarity angle denotes the angle between the carbonyl bond (C1–O1) and the plane of the chromophore phenolate ring; the angle is 90° when this bond is normal to the plane. O1 = chromophore carbonyl oxygen, O4′ = chromophore phenolate oxygen, Tyr42 = hydroxyl oxygen of Tyr42, Glu46 = $O^{\varepsilon 2}$ of Glu46, Cys69 = backbone amide nitrogen of Cys69.

Structural dynamics for *trans–cis* isomerization (BP and HT models). The refined structures of intermediates and their kinetics characterize the *trans–cis* isomerization with atomic detail. To highlight structural differences visually, colour-coded skeletal structures of pG and I_T are superimposed with I_{CT} in Fig. 5a and with pR_1 in Fig. 5b. Comparison of the white (pG) and orange (I_T) structures reveals the changes associated with the pG to I_T transition, seen most clearly in the side views. The I_T structure is highly non-planar (planarity angle of 85°) and the torsion angle of 85° around its C2–C3 bond lies between the *trans* (169° in pG) and *cis* values (−1° and 1° in I_{CT} and pR_1, respectively). Thus I_T lies on the junction of the pathways that lead from pG to I_{CT} and pR_1. The pCA chromophore becomes severely bent in which the C1′ atom of the phenolate ring acts as a pivot and the carbonyl O1 swings out of the plane of the phenolate moiety. I_T bifurcates along two pathways to produce

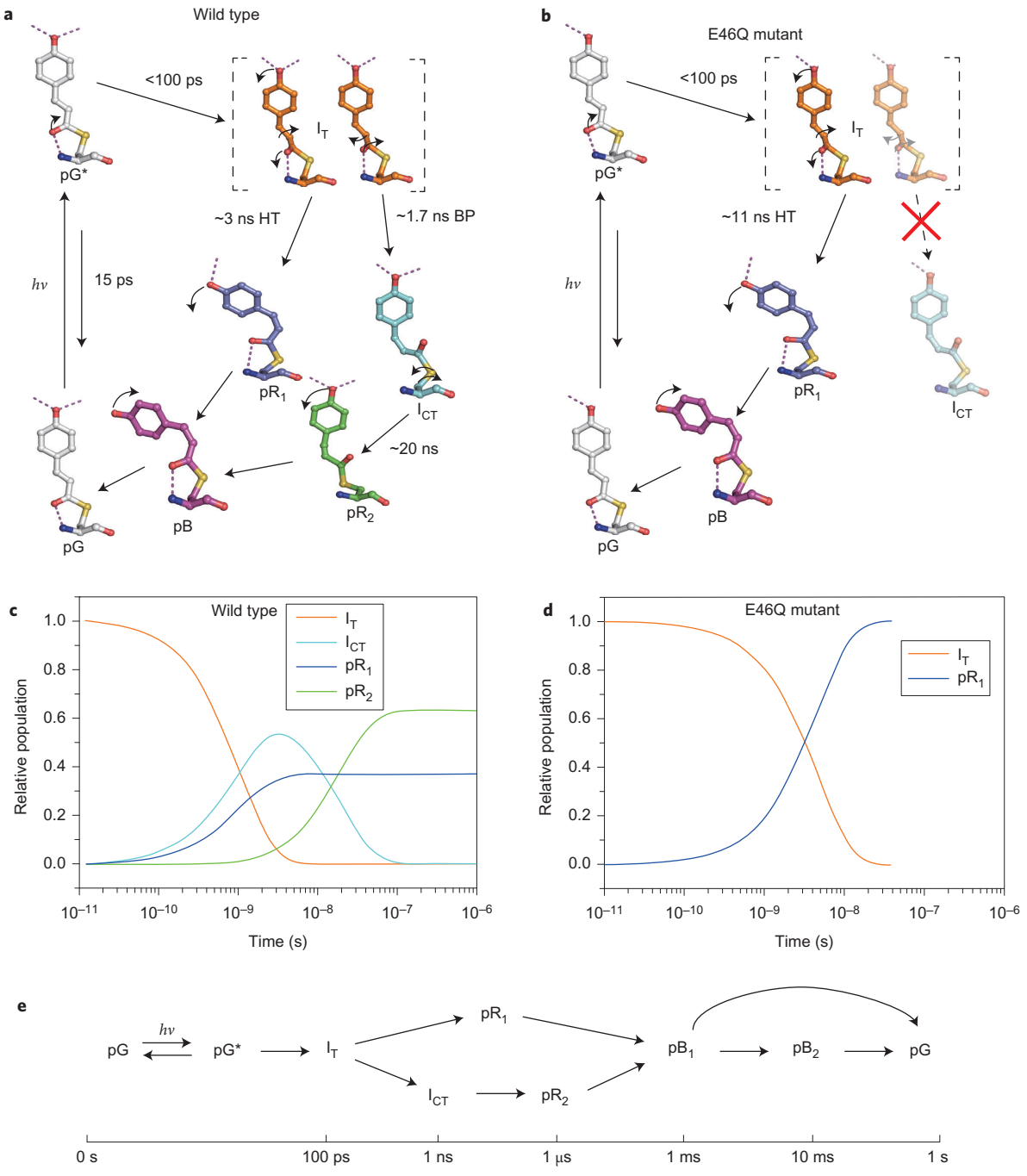

Figure 4 | Structures of pCA intermediates, reaction pathways and kinetics. a, A photocycle consistent with WT-PYP time-resolved electron-density maps. Carbon atoms of the refined pG, I_T, I_{CT}, pR_1 and pR_2 intermediate structures are shown in grey, orange, cyan, dark blue and green, respectively. Oxygen, sulfur and nitrogen atoms are shown in red, yellow and blue, respectively, and the arrows indicate significant atomic movement from one intermediate to the next. **b**, A photocycle consistent with the E46Q-PYP density maps. All the colour schemes are identical to those in (**a**). The pathway from I_T to I_{CT} via the BP mechanism is blocked because of the weaker hydrogen bond between pCA and Q46. **c**, Time-dependent concentrations of intermediates consistent with (**a**), with the colour code as in (**a**). The solid lines are from the posterior analysis with time constants $\tau_1 = 1.7$ ns, $\tau_2 = 3$ ns and $\tau_3 = 20$ ns. **d**, Time-dependent concentrations of intermediates consistent with (**b**), with the colour code as in (**a**). The solid lines are from the posterior analysis with a time constant $\tau_1 = 11$ ns. **e**, The reaction pathways of the entire photocycle of WT-PYP. The reaction pathways for late time delays that involve pB states and their return to pG are adopted from previous studies[17,33].

two different *cis* intermediates (I_{CT} and pR_1) via the BP and HT pathways, respectively. The isomerization trajectory that leads to pR_1 occurs via the HT mechanism (left-most pathway in Fig. 4a; see also Fig. 5b), in which the carbonyl O1 returns to the same side of the ground-state chromophore as in the ground-state pG by breaking the hydrogen bond between the phenolate oxygen and Glu46; the pCA again becomes planar. Isomerization to I_{CT} occurs via the BP mechanism (right-most pathway in Fig. 4a; see also Fig. 5a), in which the carbonyl O1 completes its excursion to the opposite side of the chromophore by breaking the hydrogen bond between O1 and the backbone amide of Cys69, and the pCA still remains highly bent. I_{CT} evolves further to generate pR_2 via another BP-like rotation about the single bonds flanking the sulfur atom. The Cruickshank Diffraction Precision Index values

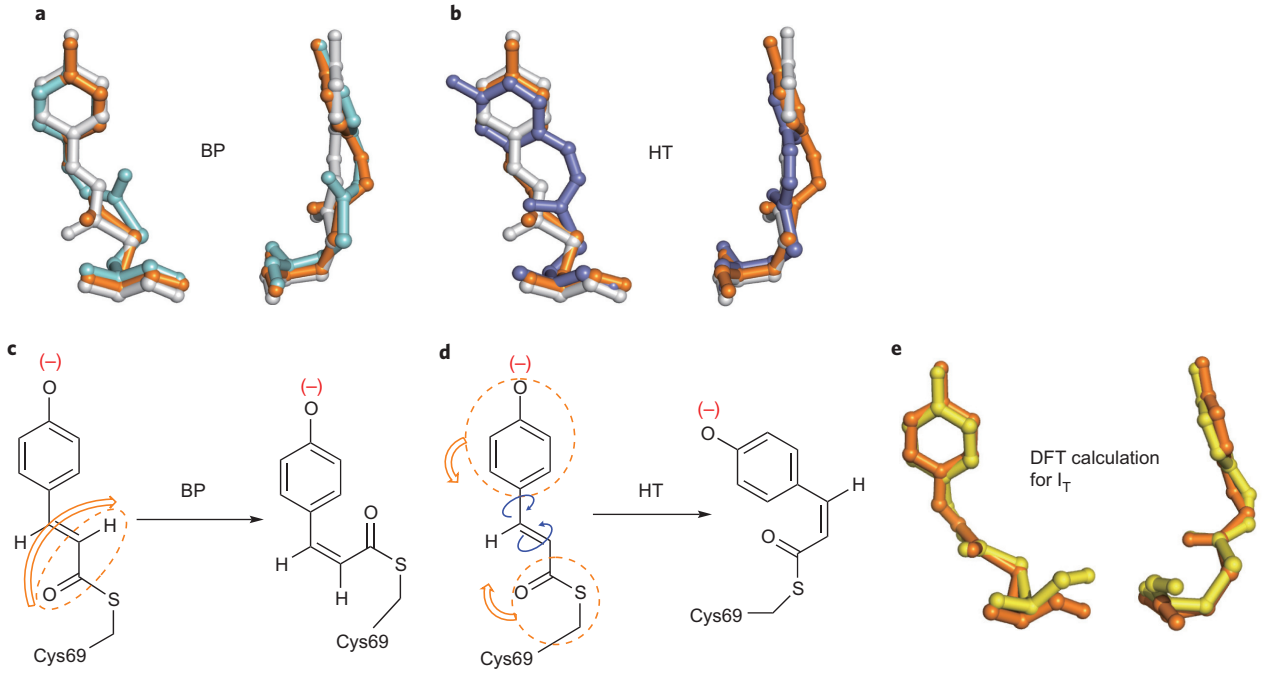

Figure 5 | HT and BP pathways and a comparison of experimental and theoretical I_T structures. a, Front and side views of the pCA structural transformation according to the BP pathway (pG → I_T → I_{CT}). **b**, The same as in (**a**), but according to the HT pathway (pG → I_T → pR_1). Movies of both pathways are shown side-by-side in Supplementary Movie S4. **c**,**d**, Schematic representation of the BP (**c**) and HT mechanisms (**d**). The bond rotations are shown with blue arrows and the orange arrows show the general movements in space of the circled sections of the molecules. **e**, Comparison of the experimental I_T structure (orange) with an energy-minimized structure (yellow) computed using DFT (B97-1/6-31G(d) + 3-21G). The residues included for stabilization are not shown for clarity (see the Supplementary Information for details).

and B-factors in Supplementary Tables S4–S6 show that these structural changes associated with the BP and HT pathways are most certainly significant. As reported in a previous nanosecond time-resolved crystallographic study[17], the structures denoted pR_1 and pR_2 are populated in a ratio of ~4:6, and both ultimately convert to pB, the long-lived, putative signalling state. The coexistence of pR_1 and pR_2 is also consistent with recent studies with pH-dependent time-resolved X-ray crystallography[32] and pump-probe X-ray solution scattering[33]. The reaction pathways of the entire photocycle for WT-PYP can be summarized as shown in Fig. 4e.

The isomerization pathway within the chromophore binding pocket that constitutes a 'protein cage' is quite different from that in the gas phase, where chromophores are free from host constraints and may isomerize via a geometrically simpler pathway, the one-bond flip[34]. Surprisingly, both the BP and HT pathways (Fig. 5a,b) appear to be operative in the protein cage, although they eventually converge to the same signalling state, pB (Fig. 4a,e). Although a kinetic model that contains parallel pathways was proposed in previous cryogenic[35] and room-temperature[36] spectroscopic studies, the three-dimensional structures could not be determined and the BP and HT pathways could not be elucidated. The high non-planarity of I_T and its unusual C1–C2–C3–C1′ torsion angle that lies between the *trans* and *cis* values indicate that I_T resembles closely a highly strained transition state. Specific hydrogen bonds and hydrophobic interactions between the pCA chromophore and the protein cage could stabilize such a structure, which could not exist in a stable form in a solvent cage or gas phase that lacks such structurally specific interactions[37,38]. Indeed, density functional theory (DFT) calculations (see the Supplementary Information) show that the optimized I_T structure (Fig. 5e) has no imaginary vibrational frequency when interactions that involve Cys69, Tyr42, Glu46, Thr50, Arg52, Ala67, Thr70 and Phe96 are included, and thus suggest that the I_T structure is stabilized as an intermediate rather than in a transition state. I_T forms on a time scale much shorter than the time resolution available in this study, so the possibility that I_T is a mixture of multiple intermediates cannot be ruled out. However, the DFT result supports strongly our interpretation of I_T as a single intermediate. In the case of the E46Q mutant, the BP pathway becomes unfavourable because the hydrogen bond to Gln46 is both longer[39] and weaker than that to Glu46, and only the HT pathway through I_T and pR_1 is operative (Fig. 4b,d). Evidently, the bifurcated pathway of isomerization within the protein cage can be redirected by modifying a single hydrogen bond.

During the preparation of the final version of this article, we became aware of an article[40] in which the photoisomerization of PYP was studied with the same techniques applied to WT-PYP crystals grown under rather different conditions, in a high salt concentration (1.1 M NaCl) and D_2O. The first intermediate reported in that article is similar to I_T, but in structure refinement the torsion angles around C2=C3 were restrained in the *cis* configuration whereas we released such constraints gradually. The first intermediate does not bifurcate into two *cis* intermediates and the HT pathway was not observed. The second intermediate is similar to I_{CT}, but is more planar and thus more closely resembles I_{CP}[17].

Structure of intermediates and comparison with previous experimental observations. Cryogenic crystallographic studies[13–15] generally trap a mixture of chromophore structures that cannot be represented accurately by a single structure. Even if individual chromophore structures are dissected from this mixture[15], these structures are distorted substantially in their central C1–C2=C3–C1′ ethylene moiety, and the carbonyl oxygen is rotated towards the opposite side of the chromophore. Compared with cryogenic structures, the unusual I_T structure found here possesses distinct characteristics. The ethylene moiety is more distorted and lies further out of the chromophore plane than in the cryogenic structures[13–15] (see the C1–C2=C3–C1′ dihedral angle in Table 1).

Its high non-planarity accompanies translocation of the electronic charge from the phenolate oxygen to the C2=C3 ethylene bond[41]. The pCA carbonyl is rotated nearly 90° relative to its resting state and the hydrogen bond between the carbonyl oxygen and the backbone amide of Cys69 is maintained, which indicates a similar strength of hydrogen bond. As the phenolate ring in I_T is displaced in a direction opposite to the C2=C3 movement, the hydrogen bonds between the phenolate oxygen and Tyr42 and Glu46 are weakened slightly, but remain intact (see Table 1). These structural characteristics indicate that I_T is analogous to a previously predicted[10,11,42,43] twisted structure that resembles the structure of a transition state. For example, femtosecond infrared spectroscopic studies[10,11] hinted at subnanosecond structural changes that involve central C2=C3 ethylene-bond distortion, carbonyl group movement, a weakened hydrogen bond to Cys69 and phenolate ring movement. MD simulations[42,44,45] of PYP after photoexcitation also suggest a distorted structure of the chromophore, in which the central C=C double-torsion angle is predicted to be close to 90°. A low-temperature infrared study[24] identified an early cryogenic intermediate (denoted PYP_H) in which the carbonyl O1 rotation is incomplete, again consistent with a major structural feature of I_T.

The position of the C1–C2=C3–C1′ ethylene moiety in I_{CT} is similar to that in the I_T structure, and the two hydrogen bonds with Ty42 and Glu46 of I_{CT} are maintained as in I_T (see Table 1), but the carbonyl O1 in I_{CT} has completed its full rotation to the opposite side. These structural aspects of I_{CT} are consistent with the spectrum that appears on the nanosecond time scale and is assigned to I_1 in femtosecond infrared studies[10,11]. Cryocrystallographic studies that target the early intermediates[13–15] and nanosecond time-resolved[17] crystallography identified essentially one structure (denoted PYP_B[14] or I_{CP}[15,17]) that resembles I_{CT} in that the carbonyl group is rotated completely and the hydrogen bonds with Tyr42 and Glu46 remain intact. However, the central C1–C2=C3–C1′ ethylene moiety is distorted in I_{CT}, which makes the chromophore in I_{CT} highly non-planar, whereas this moiety in PYP_B[14] and I_{CP}[15] is planar. The time resolution of the nanosecond time-resolved crystallography study[17] did not allow the I_T structure to be captured. The density map at the earliest time delay (1 ns) was assigned to a single structure denoted I_{CP}, which nevertheless did not account fully for all the density, leaving some unexplained residual density (see the Supplementary Information for further discussion).

The pR_1 structure here is identical to that of pR_{E46Q} identified in a previous nanosecond time-resolved study[17]. Unlike I_{CT}, which retains its hydrogen bonds to Tyr42 and Glu46, the chromophore in pR_1 maintains only its hydrogen bonds to Tyr42 and the backbone amide of Cys69, but loses its hydrogen bond to Glu46. A second pR-like intermediate (pR_2), with a structure identical to that of pR_{CW} identified in a previous cryocrystallographic study[15] and with time-resolved crystallography[17,32], is produced from I_{CT} via another BP-like rotation about the bonds connected to the Cys69 sulfur atom. The sulfur atom remains stationary in I_T, I_{CT} and pR_1, but moves significantly in pR_2. Movement of the sulfur atom subsequent to C=O rotation is consistent with MD simulations[42].

Time-resolved ultraviolet/visible spectroscopy studies[24,46] reported that a spectroscopic intermediate, denoted I_0, decayed with a lifetime of 220 ps to another, denoted $I_0^{\ddagger}$, which decayed to I_1 with a lifetime of 3 ns. To account for the time constants, we can assign the spectroscopic intermediate I_0 to the structure I_T, $I_0^{\ddagger}$ to a mixture of the two structures I_{CT} and pR_1, and I_1 to a mixture of pR_1 and pR_2. Ultrafast vibrational spectroscopy studies[10–12] at ambient temperature, which afford sensitivity to transient stretching modes of the chromophore and protein residues, identified only I_0 and I_1 intermediates in the subnanosecond and nanosecond time regime. In addition, femtosecond infrared spectroscopy studies[10,11] detected a new intermediate (GSI) that forms on a femtosecond time scale and decays to the ground state with a time constant of 6 ps. The current time resolution of ~100 ps does not allow us to capture the GSI. According to the femtosecond infrared results[10,11], as reflected in the Glu46 C=O mode, the hydrogen bond between Glu46 and the chromophore may change slightly in strength during the I_0 to I_1 transition with a subnanosecond time constant. In our mechanism, I_T retains the hydrogen bond to Glu46 and then converts into a mixture of I_{CT} and pR_1. The hydrogen bond to Glu46 is broken in pR_1 but is intact in I_{CT}, so the infrared signal associated with the Glu46 C=O mode should be sensitive to the conversion of I_T into pR_1, but not to the conversion of I_T into I_{CT}. In addition, the subsequent conversion of I_{CT} into pR_2 may also escape detection by infrared spectroscopy, because the movement of the sulfur atom ($C1–S_\gamma–C_\beta–C_\alpha$) does not exhibit a clear spectral signature. These results suggest that I_0 and I_1 from the infrared studies can be identified with I_T and a mixture of I_{CT}, pR_1 and pR_2, respectively. Nearby residues, such as Arg52, Phe96 and Met100, within the protein pocket move substantially to accommodate the twisted structure of I_T and move further in the transition from I_T to subsequent intermediates (I_{CT}, pR_1 and pR_2; see Fig. 2, Supplementary Figs S1–S3 and Supplementary Movies S1–S3). Transient infrared spectra seem to be less sensitive to movement of these residues[12].

Conclusions

Time-resolved Laue crystallography has unveiled for the first time a long-hypothesized highly twisted intermediate along the *trans*-to-*cis* isomerization pathway. This structure is crucial for the proper interpretation of results from computational studies and time-resolved spectroscopic studies. The detailed structures of intermediates and their dynamics provide insights that tie together and help reconcile previous experimental observations from various techniques. That the lifetime of the I_T intermediate is sufficiently long to be resolved with a 100 ps time resolution is testimony to the specific, highly stabilizing interplay between the pCA chromophore and the protein cage that surrounds it. The detailed structural transitions indicate that the hydrogen bonds between the chromophore and the surrounding side chains play important roles; indeed, the number of hydrogen bonds progressively decreases as the reaction proceeds. The I_T intermediate acts as the gate, bifurcating into two different *cis* intermediates, and reaction pathways can be controlled by modifying the environment of the chromophore.

Methods

Data collection protocol. Time-resolved Laue diffraction images were acquired at beamline ID09B at the European Synchrotron Radiation Facility (ESRF) and at BioCARS beamline 14-IDB at the Advanced Photon Source (APS) using the pump-probe method: a laser pulse triggered a photochemical reaction in a PYP crystal (pump) and a time-delayed X-ray pulse produced a diffraction pattern on a Mar165 CCD detector (probe). The excitation laser pulse was generated by stretching 400 nm, ~120 fs pulses to ~100 ps via a silica rod and optical fibre (for ESRF) or by tuning the femtosecond-pulse train of 780 nm pulses to ~35 ps of 390 nm laser pulses via the TOPAS optical parametric amplifier and echelon (for APS). To maximize the number of X-ray photons in a single-probe pulse, the experiment was scheduled in a four-bunch mode (ESRF) or a hybrid mode (APS). Diffraction images were acquired at all the desired time delays before rotating the crystal to a new angular setting. Numerous orientations, each of which sampled a different region of reciprocal space, could be acquired from each rod-shaped PYP crystal. The time series consisted of a negative time point (−20 ns) and several positive time points (from 0 ps to 1 μs).

Data processing. The data are highly redundant and the resolution cut-off extends below 1.6 Å. Indexing, integration, scaling and merging of all the data sets was performed with LaueView[46] and yielded the structure factor amplitudes ($|\mathbf{F}(hkl, t)|$) and the associated errors ($\sigma(hkl)$) for each reflection and time point. The values of $|\mathbf{F}(hkl, \text{reference})|$ were used to represent the amplitude of the dark state. The reference time point corresponds to a negative time delay or a laser-off condition.

The time-dependent difference structure-factor amplitudes were obtained by scaling to calculated (absolute) amplitudes from the ground-state structure (F_c^{dark}) and by subtraction: $\Delta F(hkl, t) = |\mathbf{F}(hkl, t)| - |\mathbf{F}(hkl, \text{reference})|$. Weighted-difference structure-factor amplitudes were generated by scaling $\Delta F(hkl, t)$ by a weight factor $w(hkl) = 1/(1 + (\Delta F(hkl)^2/ < \Delta F^2 >) + (\sigma(hkl)^2/ < \sigma^2 >))$ (ref. 16). Weighted-difference structure factors ($w(hkl) \times \Delta F(hkl, t)$) from different volumes on a single crystal and from multiple crystals were merged to produce a single highly redundant and complete data set at each time point.

SVD analysis. To identify the kinetic mechanism and the structure of intermediates during the early time photocycle of PYP, we extracted time-independent difference electron densities from the mixture of time-dependent densities at each time point using the method of SVD[31]. The SVD results show that only the first three lSVs (for WT-PYP) or the first two lSVs (for E46Q-PYP) have significant singular values and positive autocorrelation factors. Linear combinations of these lSVs reproduced the experimental data with high fidelity. To extract the time-independent difference electron-density maps, we performed kinetic analyses using a simple three-state (for WT-PYP) or two-state (for E46Q-PYP) sequential model. Assuming a simple kinetic pathway that involves three (for WT-PYP) or two (for E46Q-PYP) states, three (for WT-PYP) or two (for E46Q-PYP) time-independent electron-density maps for three (for WT-PYP) or two (for E46Q-PYP) intermediates can be constructed from simple linear combinations of the three (for WT-PYP) or two (for E46Q-PYP) components with refined time constants (see the Supplementary Information for details). The time-independent difference maps recovered from SVD analysis (Fig. 3) were used to refine the time-independent structures.

Structure refinement. All refinements and the model building were performed with SHELX-97[47] and XtalView[48] (Fig. 3). Of the total reflections, 5% were used to calculate a free *R*-factor. The refinement of intermediate structures was performed against electron-density maps that had been extrapolated to 100% photoactivation. The structures of three intermediates for WT-PYP were refined against the three data sets of time-independent extrapolated structure factor amplitudes. The first of the three extrapolated maps is structurally homogeneous; that is, it is modelled well by a single structure (I_T). The second map is structurally heterogeneous, which suggests a mixture of two distinct intermediates, and refinement employed a mixture of two structures ($I_{CT} + pR_1$). The third map is also structurally heterogeneous and was refined using a mixture of pR_1 and pR_2. For E46Q-PYP, the structures of two intermediates were refined against the two time-independent extrapolated structure factor amplitudes. Both maps are structurally homogeneous and the first and second maps were modelled by I_T and pR_1, respectively. The values of the *R* (*R*-free) factor in Supplementary Tables S4–S6 represent a structure refinement of good quality.

Posterior analysis. To explore kinetic mechanisms consistent with our data, posterior analysis[17,31] was applied with time-independent difference density maps, which were derived from previously refined intermediate structures (I_T, I_{CT}, pR_1 and pR_2). We had determined the time-independent mixture of these two structures previously, so we explored a bifurcation mechanism in which the first intermediate, I_T, converts into I_{CT} and pR_1 (and subsequently I_{CT} further transforms into pR_2; Fig. 4). The fit between these calculated difference density maps and the experimental difference density maps resulted in three (for WT-PYP) or one (for E46Q-PYP) associated time constants (see the Supplementary Information for details).

Protein Data Bank codes. Atomic coordinates and structure factor amplitudes are deposited in the Protein Data Bank under accession codes 3VE3 (I_T), 3VE4 ($I_{CT} + pR_1$), and 4HY8 ($pR_1 + pR_2$) for WT-PYP, ESRF; 4I38 (I_T), 4I39 ($I_{CT} + pR_1$), and 4I3A ($pR_1 + pR_2$) for WT-PYP, APS; 4I3I (I_T) and 4I3J (pR_1) for E46Q-PYP, APS.

Received 10 July 2012; accepted 19 December 2012; published online 3 February 2013

References

1. Liu, R. S. & Asato, A. E. The primary process of vision and the structure of bathorhodopsin: a mechanism for photoisomerization of polyenes. *Proc. Natl Acad. Sci. USA* **82,** 259–263 (1985).
2. Warshel, A. & Barboy, N. Energy storage and reaction pathways in the first step of the vision process. *J. Am. Chem. Soc.* **104,** 1469–1476 (1982).
3. Muller, A. M., Lochbrunner, S., Schmid, W. E. & Fuss, W. Low-temperature photochemistry of previtamin D: a hula-twist isomerization of a triene. *Angew. Chem. Int. Ed.* **37,** 505–507 (1998).
4. Liu, R. S., Yang, L. Y. & Liu, J. Mechanisms of photoisomerization of polyenes in confined media: from organic glasses to protein binding cavities. *Photochem. Photobiol.* **83,** 2–10 (2007).
5. Imamoto, Y., Kataoka, M. & Liu, R. S. Mechanistic pathways for the photoisomerization reaction of the anchored, tethered chromophore of the photoactive yellow protein and its mutants. *Photochem. Photobiol.* **76,** 584–589 (2002).
6. Andruniow, T., Ferre, N. & Olivucci, M. Structure, initial excited-state relaxation, and energy storage of rhodopsin resolved at the multiconfigurational perturbation theory level. *Proc. Natl Acad. Sci. USA* **101,** 17908–17913 (2004).
7. Frutos, L. M., Andruniow, T., Santoro, F., Ferre, N. & Olivucci, M. Tracking the excited-state time evolution of the visual pigment with multiconfigurational quantum chemistry. *Proc. Natl Acad. Sci. USA* **104,** 7764–7769 (2007).
8. Schapiro, I., Weingart, O. & Buss, V. Bicycle-pedal isomerization in a rhodopsin chromophore model. *J. Am. Chem. Soc.* **131,** 16–17 (2009).
9. Xie, A., Hoff, W. D., Kroon, A. R. & Hellingwerf, K. J. Glu46 donates a proton to the 4-hydroxycinnamate anion chromophore during the photocycle of photoactive yellow protein. *Biochemistry* **35,** 14671–14678 (1996).
10. van Wilderen, L. J. *et al.* Ultrafast infrared spectroscopy reveals a key step for successful entry into the photocycle for photoactive yellow protein. *Proc. Natl Acad. Sci. USA* **103,** 15050–15055 (2006).
11. Groot, M. L. *et al.* Initial steps of signal generation in photoactive yellow protein revealed with femtosecond mid-infrared spectroscopy. *Biochemistry* **42,** 10054–10059 (2003).
12. Heyne, K. *et al.* Structural evolution of the chromophore in the primary stages of *trans*/*cis* isomerization in photoactive yellow protein. *J. Am. Chem. Soc.* **127,** 18100–18106 (2005).
13. Genick, U. K., Soltis, S. M., Kuhn, P., Canestrelli, I. L. & Getzoff, E. D. Structure at 0.85 Å resolution of an early protein photocycle intermediate. *Nature* **392,** 206–209 (1998).
14. Kort, R., Hellingwerf, K. J. & Ravelli, R. B. Initial events in the photocycle of photoactive yellow protein. *J. Biol. Chem.* **279,** 26417–26424 (2004).
15. Anderson, S., Srajer, V. & Moffat, K. Structural heterogeneity of cryotrapped intermediates in the bacterial blue light photoreceptor, photoactive yellow protein. *Photochem. Photobiol.* **80,** 7–14 (2004).
16. Ren, Z. *et al.* A molecular movie at 1.8 Å resolution displays the photocycle of photoactive yellow protein, a eubacterial blue-light receptor, from nanoseconds to seconds. *Biochemistry* **40,** 13788–13801 (2001).
17. Ihee, H. *et al.* Visualizing reaction pathways in photoactive yellow protein from nanoseconds to seconds. *Proc. Natl Acad. Sci. USA* **102,** 7145–7150 (2005).
18. Andresen, M. *et al.* Structure and mechanism of the reversible photoswitch of a fluorescent protein. *Proc. Natl Acad. Sci. USA* **102,** 13070–13074 (2005).
19. Sprenger, W. W., Hoff, W. D., Armitage, J. P. & Hellingwerf, K. J. The eubacterium *Ectothiorhodospira halophila* is negatively phototactic, with a wavelength dependence that fits the absorption spectrum of the photoactive yellow protein. *J. Bacteriol.* **175,** 3096–3104 (1993).
20. Borgstahl, G. E., Williams, D. R. & Getzoff, E. D. 1.4 Å structure of photoactive yellow protein, a cytosolic photoreceptor: unusual fold, active site, and chromophore. *Biochemistry* **34,** 6278–6287 (1995).
21. Ujj, L. *et al.* New photocycle intermediates in the photoactive yellow protein from *Ectothiorhodospira halophila*: picosecond transient absorption spectroscopy. *Biophys. J.* **75,** 406–412 (1998).
22. Hoff, W. D. *et al.* Measurement and global analysis of the absorbance changes in the photocycle of the photoactive yellow protein from *Ectothiorhodospira halophila*. *Biophys. J.* **67,** 1691–1705 (1994).
23. Brudler, R., Rammelsberg, R., Woo, T. T., Getzoff, E. D. & Gerwert, K. Structure of the I_1 early intermediate of photoactive yellow protein by FTIR spectroscopy. *Nature Struct. Biol.* **8,** 265–270 (2001).
24. Imamoto, Y. *et al.* Low-temperature Fourier transform infrared spectroscopy of photoactive yellow protein. *Biochemistry* **40,** 8997–9004 (2001).
25. Devanathan, S. *et al.* Femtosecond spectroscopic observations of initial intermediates in the photocycle of the photoactive yellow protein from *Ectothiorhodospira halophila*. *Biophys. J.* **77,** 1017–1023 (1999).
26. Unno, M., Kumauchi, M., Hamada, N., Tokunaga, F. & Yamauchi, S. Resonance Raman evidence for two conformations involved in the L intermediate of photoactive yellow protein. *J. Biol. Chem.* **279,** 23855–23858 (2004).
27. Takeshita, K., Imamoto, Y., Kataoka, M., Tokunaga, F. & Terazima, M. Themodynamic and transport properties of intermediate states of the photocyclic reaction of photoactive yellow protein. *Biochemistry* **41,** 3037–3048 (2002).
28. Schmidt, M. *et al.* Protein kinetics: structures of intermediates and reaction mechanism from time-resolved X-ray data. *Proc. Natl Acad. Sci. USA* **101,** 4799–4804 (2004).
29. Rajagopal, S. *et al.* A structural pathway for signaling in the E46Q mutant of photoactive yellow protein. *Structure* **13,** 55–63 (2005).
30. Schotte, F. *et al.* Watching a protein as it functions with 150-ps time-resolved X-ray crystallography. *Science* **300,** 1944–1947 (2003).
31. Schmidt, M., Rajagopal, S., Ren, Z. & Moffat, K. Application of singular value decomposition to the analysis of time-resolved macromolecular X-ray data. *Biophys. J.* **84,** 2112–2129 (2003).
32. Tripathi, S., Srajer, V., Purwar, N., Henning, R. & Schmidt, M. pH dependence of the photoactive yellow protein photocycle investigated by time-resolved crystallography. *Biophys. J.* **102,** 325–332 (2012).
33. Kim, T. W. *et al.* Protein structural dynamics of photoactive yellow protein in solution revealed by pump-probe X-ray solution scattering. *J. Am. Chem. Soc.* **134,** 3145–3153 (2012).
34. Liu, R. S. & Hammond, G. S. The case of medium-dependent dual mechanisms for photoisomerization: one-bond-flip and hula-twist. *Proc. Natl Acad. Sci. USA* **97,** 11153–11158 (2000).

35. Imamoto, Y., Kataoka, M. & Tokunaga, F. Photoreaction cycle of photoactive yellow protein from *Ectothiorhodospira halophila* studied by low-temperature spectroscopy. *Biochemistry* **35,** 14047–14053 (1996).
36. Imamoto, Y., Kataoka, M., Tokunaga, F., Asahi, T. & Masuhara, H. Primary photoreaction of photoactive yellow protein studied by subpicosecond–nanosecond spectroscopy. *Biochemistry* **40,** 6047–6052 (2001).
37. Ryan, W. L., Gordon, D. J. & Levy, D. H. Gas-phase photochemistry of the photoactive yellow protein chromophore *trans-p*-coumaric acid. *J. Am. Chem. Soc.* **124,** 6194–6201 (2002).
38. Espagne, A., Paik, D. H., Changenet-Barret, P., Martin, M. M. & Zewail, A. H. Ultrafast photoisomerization of photoactive yellow protein chromophore analogues in solution: influence of the protonation state. *ChemPhysChem* **7,** 1717–1726 (2006).
39. Sugishima, M. *et al.* Structure of photoactive yellow protein (PYP) E46Q mutant at 1.2 Å resolution suggests how Glu46 controls the spectroscopic and kinetic characteristics of PYP. *Acta Crystallogr.* **D60,** 2305–2309 (2004).
40. Schotte, F. *et al.* Watching a signaling protein function in real time via 100-ps time-resolved Laue crystallography. *Proc. Natl Acad. Sci. USA* **109,** 19256–19261 (2012).
41. Premvardhan, L. L., van der Horst, M. A., Hellingwerf, K. J. & van Grondelle, R. Stark spectroscopy on photoactive yellow protein, E46Q, and a nonisomerizing derivative, probes photo-induced charge motion. *Biophys. J.* **84,** 3226–3239 (2003).
42. Groenhof, G. *et al.* Photoactivation of the photoactive yellow protein: why photon absorption triggers a *trans*-to-*cis* isomerization of the chromophore in the protein. *J. Am. Chem. Soc.* **126,** 4228–4233 (2004).
43. Espagne, A. *et al.* Ultrafast light-induced response of photoactive yellow protein chromophore analogues. *Photochem. Photobiol. Sci.* **6,** 780–787 (2007).
44. Henry, E. R. The use of matrix methods in the modeling of spectroscopic data sets. *Biophys. J.* **72,** 652–673 (1997).
45. Boggio-Pasqua, M., Robb, M. A. & Groenhof, G. Hydrogen bonding controls excited-state decay of the photoactive yellow protein chromophore. *J. Am. Chem. Soc.* **131,** 13580–13581 (2009).
46. Ren, Z. & Moffat, K. Quantitative analysis of synchrotron Laue diffraction patterns in macromolecular crystallography. *J. Appl. Crystallogr.* **28,** 461–481 (1995).
47. Sheldrick, G. M. A short history of SHELX. *Acta Crystallogr. A* **64,** 112–122 (2008).
48. McRee, D. E. XtalView/Xfit – a versatile program for manipulating atomic coordinates and electron density. *J. Struct. Biol.* **125,** 156–165 (1999).
49. Devanathan, S., Lin, S., Cusanovich, M. A., Woodbury, N. & Tollin, G. Early intermediates in the photocycle of the Glu46Gln mutant of photoactive yellow protein: femtosecond spectroscopy. *Biophys. J.* **79,** 2132–2137 (2000).

Acknowledgements

We acknowledge extensive support from M. Wulff of beamline ID09 at ESRF during data collection there. We thank M. Wulff, P. Anfinrud, F. Schotte and H. S. Cho for their earlier contributions to this research. This work was supported by the Research Center Program (CA1201) of Institute for Basic Science (IBS) in Korea and by Creative Research Initiatives (Center for Time-Resolved Diffraction) of MEST/NRF of Korea. M.S. is supported by National Science Foundation grants 0952643 (Career) and 0843459. K.M. is supported by National Institutes of Health (NIH) grant GM036452. Use of the BioCARS Sector 14 at the APS was supported by NIH National Institute of General Medical Sciences grant P41GM103543. The time-resolved set up at Sector 14 was funded in part through collaboration with P. Anfinrud (NIH/NIDDK) through the Intramural Research Program of the NIDDK. Use of the APS was supported by the US Department of Energy, Basic Energy Sciences, Office of Science, under Contract No. DE-AC02-06CH11357.

Author contributions

H.I. designed the study, and Y.O.J. and H.I. purified, crystallized, collected and analysed the X-ray data. V.S. helped with the analysis of the X-ray data. Y.O.J., J.H.L. and M.S. performed the kinetic analysis of time-dependent data. J.K. performed the DFT calculations. Y.O.J., K.M. and H.I. co-wrote the paper. All the authors discussed the results and commented on the manuscript.

Additional information

Supplementary information is available in the online version of the paper. Reprints and permission information is available online at http://www.nature.com/reprints. Correspondence and requests for materials should be addressed to H.I.

Competing financial interests

The authors declare no competing financial interests.